Journal of Magnetic Resonance 202 (2010) 1–8

Contents lists available at ScienceDirect

Journal of Magnetic Resonance

journal homepage: www.elsevier.com/locate/jmr

Measurements of magnetic field stability in inhomogeneous magnetic fields at low temperature

Cedric Hugon [a], Jacques-Francois Jacquinot [b], Dimitris Sakellariou [a,*]

[a] CEA, DSM, IRAMIS, SIS2M, LSDRM, CEA Saclay, F-91191 Gif-sur-Yvette, France
[b] CEA, DSM, IRAMIS, SPEC, CEA Saclay, F-91191 Gif-sur-Yvette, France

ARTICLE INFO

Article history:
Received 6 April 2009
Revised 3 August 2009
Available online 15 August 2009

Keywords:
NMR
Field stability
Liquid ^{3}He
Inhomogeneous field
Inductive coupling

ABSTRACT

We present an original method for field stability measurements in a bath of liquid helium. This method is used to validate the power supply of a superconductive magnet operating in driven mode. The experiment consists in the measurement of the NMR signal of a sample of liquid ^{3}He, placed inside the field of a test magnet driven by a power supply. The homogeneity of the magnet is a strongly limiting factor for measurements but through the use of an inductively coupled microcoil and careful signal processing, a precision of 5.5 ppm was achieved.

1. Introduction

Future developments in NMR/MRI involve the use of extremely strong magnets currently unavailable. In this context, the CEA is intending to build the biggest MRI magnet ever made, an 11.75 T full body imaging system called ISEULT [1]. Given the complexity of the coil, it is expected that the magnet will not be able to work in persistent mode. As a result, a power supply is required to compensate the resistive loss in the coil.

The system is required to achieve a very high magnetic field stability on short and long term (10^{-4} ppm over 10 min and 0.05 ppm/h). As a result, the stability of the power supply and additional stabilization systems driving the magnet has to be proved. The initial test power supply is designed to provide about 1000 A with a stability of 2 ppm/h. In order to achieve a 0.05 ppm/h stability the CEA magnet designers have added to the magnet a stabilization system [2]. The purpose of the experiment is to prove that this system is effective.

The required accuracy for the field measurement was obtained using flux coils for short range variations (few seconds) but the drift of the integrator forbids long-term measurements (minutes to hours). It is well known that NMR is one of the most precise ways to measure a magnetic field. As a result, it is the method of choice for the long-term stability assessment.

The difficulty of the measurement resides in the fact that the only superconductive magnet quickly available for the experiment does not provide a room-temperature hole: The center of the magnet is filled with liquid helium which is used for cooling the superconductive coil. As a result, one must use an NMR-sensitive sample with narrow linewidth that will be cooled at liquid helium temperature. Another difficulty for this experiment is that the magnet was never designed for NMR experiments: It is highly inhomogeneous and the only possible way to limit inhomogeneity and obtain signal is by using a very small sample.

As we intend to measure a magnetic field, this experiment has different requirements from regular NMR experiments. The actual goal of the experiment is to follow the center frequency of the NMR peak that is measured, as it drifts with the field. The frequency measurement must be refreshed often to provide temporal resolution and the signal should also yield a high signal to noise with long lifetime to guarantee high frequency resolution. These requirements place constraints on the relaxation times T_1, T_2 and gyromagnetic ratio γ of the sample that will be used.

2. Experimental setup

As mentioned above, the test magnet constrains the experiment to temperatures below 3.2 K (liquid ^{4}He at atmospheric pressure). Furthermore, the magnet is highly inhomogeneous with about 200 ppm variation within a sphere of 2 mm diameter at the center of the magnet. In such conditions, in the working field we used (1.11 T), a regular NMR probe would pickup a very weak signal because of the spectral spread.

* Corresponding author. Address: CEA, Departement des Sciences de la Matiore, DSM, IRAMIS, SCM, SIS2M, LSDRM, CEA Saclay, F-91191 Gif-sur-Yvette, France.
E-mail addresses: cedric.hugon@cea.fr (C. Hugon), jacques-francois.jacquinot@cea.fr (J.-F. Jacquinot), dsakellariou@cea.fr (D. Sakellariou).

1090-7807/$ - see front matter © 2009 Elsevier Inc. All rights reserved.
doi:10.1016/j.jmr.2009.08.005

A solution to this problem is to spatially select the region of detection and reduce it to a very small volume. This can be accomplished through the use of a microcoil [3,4]. A microcoil allows the decrease of sample size while keeping a high filling factor and hence a good sensitivity. In this case, reducing the size of the sample decreases the linewidth and increases the SNR.

A high signal to noise ratio (SNR) is required to follow the center of mass (centroid) of the line. Besides, this high SNR should be obtained in a short period of time, to allow fast data refresh rate. As a result, to achieve high SNR and narrow linewidth, the choice of the sample is critical. Most hydrogen compounds are solid at liquid helium temperature and hence display large spectral width. We have experimented with some solids such as platinum but found out the resulting signal was not suitable for our purpose. These have longer T_2 but their γ is lower than for proton and results in a lower polarization (for Pt, $\gamma = 5.7505 \times 10^7$ rad T^{-1} s^{-1}, or $\frac{\gamma_H}{\gamma_{Pt}} = 4.65$). An interesting nucleus for this experiment is ^{3}He, which has a spin 1/2 and is highly sensitive $\left(\frac{\gamma_H}{\gamma_{^3He}} = -1.31\right)$. ^{3}He is however gaseous at liquid ^{4}He temperature under atmospheric pressure. As a result, its signal would be very weak. But pumping the liquid ^{4}He bath causes temperature to decrease and reach a point where ^{3}He is liquid under a certain pressure. Liquid ^{3}He is the ideal sample in this case as it provides a high signal ($\gamma = -20.378 \times 10^7$ rad T^{-1} s^{-1} and high spin density). Low and Rorschach [5] have measured T_1 and T_2 for liquid ^{3}helium under diverse conditions. At atmospheric pressure and temperatures between 2 K and 3 K, T_2 can be expected between 15 and 30 s while T_1 should be expected between 300 and 400 s. As a result, the linewidth of ^{3}He should not be a limitation, but its T_1 might be an issue in terms of repetition rate and refresh rate. It is then desirable to add paramagnetic impurities in the enclosure containing the sample to accelerate the spin–lattice relaxation. We hence rinsed the quartz cell and the coil used for the experiment with a $CuSO_4$, 1 M solution.

The conjugation of a microcoil orthogonal to the static field with liquid ^{3}He poses some technical issues. The static field being vertical, the coil has to produce a horizontal RF field B_1 (Fig. 1). We have chosen to use a solenoidal coil placed with its axis horizontally for sensitivity reasons. Besides, the dewar of the magnet is vertical and offers access only from the top. The dewar does not remain cold all the time. It is cooled down only a few hours before the experiment, after the measurement cell is placed inside. As a result, the ^{3}He has to condensate at the beginning of the experiment in the region enclosed by the coil. To ensure that the liquid properly fills the horizontal coil, we chose to have the coil actually drowned in liquid ^{3}He. To achieve this, we made a quartz cell with a specially formed bottom, in which the microcoil was placed. A volume of gaseous ^{3}He (2.15 l at atmospheric pressure) was placed outside the dewar, linked through a steel capillary (approx. 2 cm^3) to the quartz cell (approx. 20 cm^3) placed inside the dewar. The cell and the pipes were evacuated, prior to the opening of the ^{3}He volume. Once the ^{3}He was released in its circuit, the system was cooled down to reach liquid helium temperature. To achieve ^{3}He condensation, the liquid helium bath was pumped, in order to reach about 2.5 K and ensure about 500 mm^3 of liquid ^{3}He were sitting at the bottom of the cell, flooding the microcoil (vapor pressures of ^{3}He for various temperature can be found in [6]). A schematic of the ^{3}He system can be seen in Fig. 1. The condensation could be verified through the sudden apparition of a strong signal around the expected frequency while the static field was on. The working frequency was chosen at 36 MHz, in order to facilitate testing prior to the experiment. This corresponds to a field of about 1.1 T.

In order to simplify the sealing of the ^{3}He circuit, we inductively coupled the microcoil with a primary coil that was linked to the detection system. To serve this purpose, a small capacitor was added to the microcoil in order to create a resonator tuned at 36 MHz. The primary coil was also tuned at 36 MHz and the coupling was expected to be strong, achieving the over-coupling regime [7,4], due to the dramatic improvement of the Q factor of copper coils at liquid helium temperatures. A schematic of the coil setup can be seen in Fig. 2. The improvement due to temperature was actually observed from no visible coupling at room temperature to a coupling factor of about 0.014 at 3.2 K. It is interesting to note here the dramatic effect of temperature on the coupling of the coils. Such an effect could be of great use in methods such as MACS [4], as this could help tremendously the achievement of over-coupling. This could be a supplemental benefit of a MAS cryo-probe using MACS. The coupling improvement is shown in Fig. 3.

The spectrometer used is a portable spectrometer LapNMR from Tecmag with a RF amplifier Tomco (250 W, 100 kHz–30 MHz). The home made probe includes a copper Faraday cage in which is

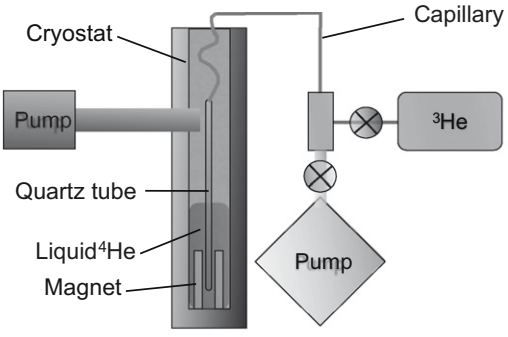

Fig. 1. Experimental setup for the ^{3}He circuit. The system provides a liquid ^{3}He sample at the bottom of the quartz cell for NMR time monitoring of the static field generated by the magnet. A tuned microcoil is placed at the bottom of the quartz cell and is inductively coupled with an external coil connected to the detection system. The circuit of ^{3}He includes a tank of 2 l of gaseous ^{3}He at atmospheric pressure. This tank is placed outside of the magnet dewar and is connected through a steel capillary to a quartz cell that plunges in the liquid helium bath used to cool the superconductive magnet. Initially, the tank is sealed and the circuit is evacuated thanks to a pump, then gaseous ^{3}He is released in the evacuated circuit and finally, the liquid helium bath is pumped in order to liquify some of the ^{3}He at the bottom of the quartz cell.

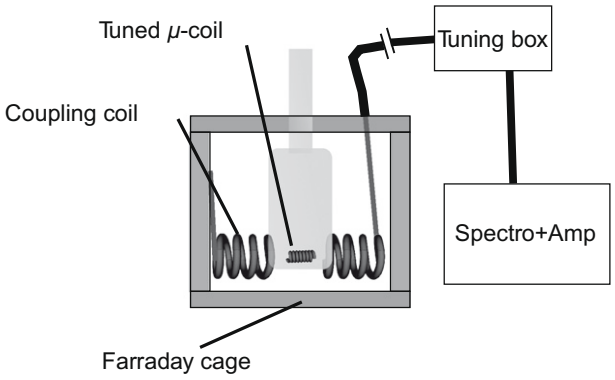

Fig. 2. Experimental setup for the detection circuit. The system detects the NMR signal of liquid ^{3}He present at the bottom of a quartz cell. A solenoidal microcoil is placed at the bottom of the quartz cell, drowned in liquid ^{3}He. This microcoil is tuned at 36 MHz with a small-sized CMS capacitor. The microcoil is inductively coupled with an external solenoidal coil that has been pulled open (split solenoid) to accommodate the cell in its center. The coils are enclosed in a grounded copper Faraday cage and the external coil is connected to the detection system (tune/match system, coupler, pre-amp and spectrometer). The ensemble is bathing in liquid ^{4}He, which is pumped in order to decrease the temperature and allow the gaseous ^{3}He to condensate inside the cell.

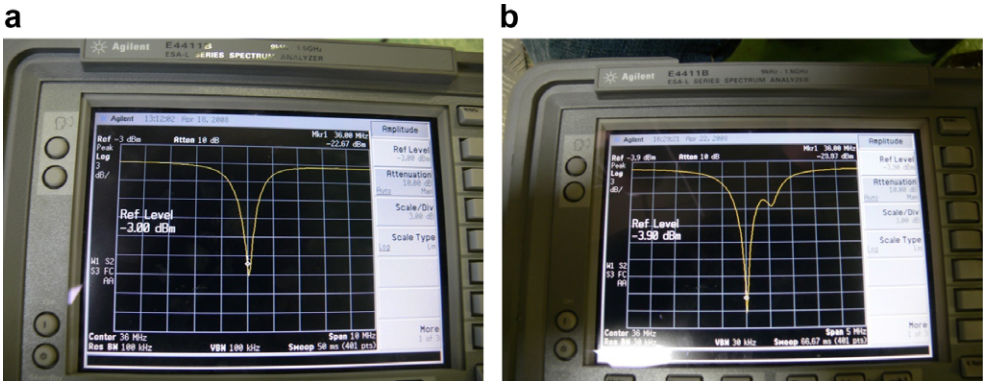

Fig. 3. (a) Resonance spectrum of the tuned circuit at room temperature. The absorption dip denotes the resonance at 36 MHz. However, the presence of a single dip indicates that the two-coil system is either under-coupled or critically coupled. Such a poor coupling is expected, given the poor geometry adopted because of the different constraints. (b) Resonance spectrum of the tuned circuit at liquid helium temperature (3.2 K). The increase of the quality factor of the coils due to the lower temperature increases the coupling of the coils, yielding a double dip indicative of the over-coupling regime.

placed the primary coil. The primary coil is a copper solenoid (0.8 mm wire)pulled open in its middle to accommodate the quartz tube. One end of the primary coil is soldered to the cage, which is grounded. The other end of this coil is linked to a tuning/matching system outside the dewar through a coaxial cable. The secondary coil is a copper solenoid (100 μm diameter wire) wound around a 1 mm diameter capillary. The capillary is removed after winding. The coil is tuned with a small-sized CMS capacitor to achieve a LC resonator centered around 36 MHz. The resonator is placed inside the quartz tube which features a specially shaped bottom that holds the coil horizontally.

3. Experimental data

The signal of cold gaseous ^{3}He was detected and the condensation could be observed through the sudden dramatic increase of SNR. For a single Hahn echo, the SNR of the gas at 4.2 K is about 25 while the SNR of the liquid at 2.5 K is about 180, that is to say an enhancement by a factor 7.2. The molar volume varies by a factor about 8.7 between the gas at 4.2 K and the liquid at 2.5 K (using ideal gas law and molar volumes for liquid ^{3}He from [6]). This can be considered in reasonable agreement given the possible variations of signal that can be due to the difference of diffusion between the gas and the liquid and the possible displacement of the coil when the liquid appears.

3.1. T_1

We first characterized the NMR signal and measured T_1 and T_2. T_1 was measured using a 2D sequence with a Hahn echo [8] in the first dimension and varying the recycle time in the second dimension. The signal was accumulated for 4 scans. The delay between the $\pi/2$ and the π pulse was 50 μs, the acquisition time for each echo was 256 μs with 26 μs between the *pi* and the beginning of the acquisition. Fig. 4 presents the amplitude of the signal for the different recycle times. The fit of the data points by an exponential yields $T_1 = 19.7$ s. This dramatic shortening of T_1 could be attributed solely to the presence of paramagnetic impurities but it is also likely that another phenomenon should be taken into account: It must be noted that the liquid is free to circulate in the coil in every direction. As a result, the self diffusion of the liquid might decrease T_1 by replacing excited spins with "new" non-excited spins located outside of the coil at the time of the pulse.

3.2. T_2

We then measured T_2 using the CPMG sequence [9,10]. The variation of the delay τ_1 between the $\frac{\pi}{2}$ and π pulse revealed a strong dependence of the apparent T_2 on the time delay between pulses τ_1. This is indicative of diffusion effects. Fig. 5 presents the time evolution of the signal amplitude for different τ_1, T_2 was found in the range from 9.3 ms to 55 ms. However, these results do not match with a standard 1D diffusion phenomenon as the diffusion occurs in three dimensions. However this does not account for the extremely high (several orders of magnitude higher) diffusion coefficient that would be found using the standard equation for a 1D diffusion process [11], given the field gradient present in the region of the coil. The apparent relaxation is most likely accelerated by the diffusion of signal-producing spins outside of the sensitive area, in the same way as T_1 is accelerated. This feature of our experiment is an important and interesting one. However, it goes beyond the scope of this paper and we will not go further on this topic.

3.3. Frequency monitoring

Given the strong signal obtained from liquid ^{3}He, full recovery of the sample magnetization was not necessary and it was possible to repeat a CPMG train as often as every 10 s. The signals of each echo of the train were summed together to enhance the SNR. The optimum SNR was obtained for a train of 60 echoes extending over approximately 25 ms. The sampling of each echo was done over 256 μs with a dwell time of 1 μs. As a result, the digital resolution was of 3906.25 Hz, that is to say about 108.5 ppm. As it is, this is obviously not sufficient to achieve the monitoring of an assumed 0.5 ppm field stability. We will see in the following sections how a much better precision can be achieved.

4. Data processing aspects

NMR monitoring of the amplitude of a magnetic field is performed by measurement of the Larmor frequency of the spins of a sample placed inside the magnetic field. This is evident from the basic Larmor formula: $f = \gamma B_0$ where γ is the gyromagnetic ratio of the nucleus studied, f the precession frequency (hence the frequency of the signal) and B_0 the static magnetic field. As a result, one is left to a problem of spectral line position monitoring. In general, with no information about the line, such a problem is the same as resolving two lines in a spectrum: The Rayleigh criterion

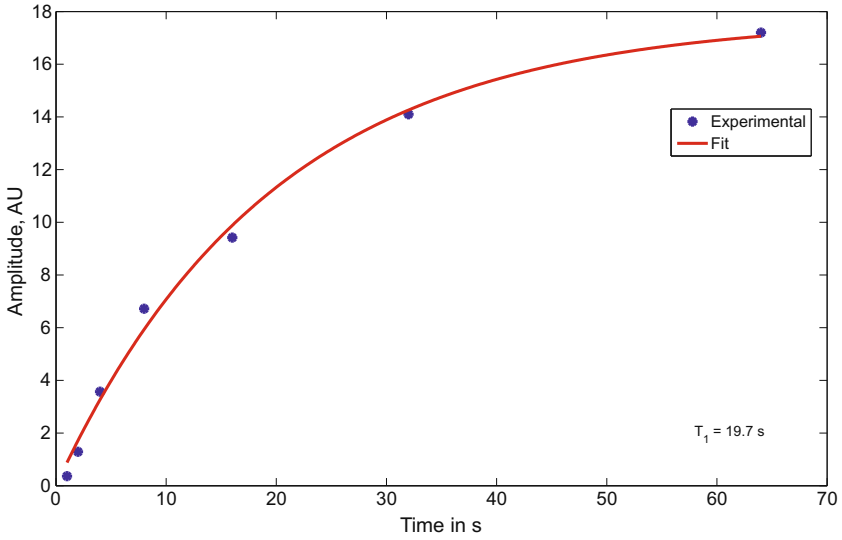

Fig. 4. Liquid ^{3}He Hahn echo signal amplitude for different recycle times after a few dummy cycles. The points are fitted with and exponential curve that yields the relaxation time T_1. T_1 is very short compared to what is reported in the literature (5 min). This can be partially explained by the presence of paramagnetic materials that we introduced in the tube before the experiment. However, it is not sufficient to explain the dramatic decrease of T_1. Most likely, diffusion in and out of the coil accelerates the relaxation by replacing excited spins with non-excited spins.

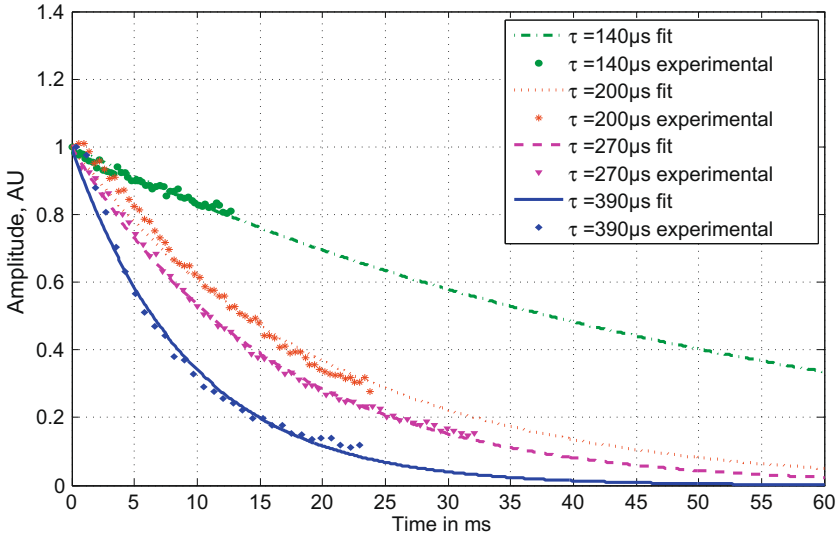

Fig. 5. Exponential fit of the envelope of the time evolution of the signal amplitude of the CPMG trains for different delays τ_1. The experimental are the amplitude of each echo and have been normalized to the first echo. The strong dependence of the relaxation time T_2 on τ_1 indicates a strong effect of diffusion. Given the expected static field gradient, this dependence is not only the result of diffusion in a gradient and the apparent T_2 is probably shortened by the diffusion of spins outside of the detection area. This same diffusion effect probably accelerates T_1 by replacing excited spins with non-excited spins.

applies and one needs the line FWHM to be as wide or narrower than the desired resolution, and one must sample the signal over a time as long as the inverse of the frequency to be resolved. In the context of multiple acquisition separated by time, if one can suppose that the lineshape never varies and only the center frequency varies, then, much more information is available and it is possible to achieve much higher precision than the digital resolution. This is basically deconvolution. In the absence of noise, one can express the line as the convolution of a reference line and a Dirac delta function. When the reference line is entirely determined and the inverse of the convolution can be computed, one can go back to the delta function and the center of the line. This assumes as mentioned before that the lineshape does not vary across the experiment. The normalized cross-correlation of each measured signal with the first acquired signal was computed in order to assess the validity of this postulate. It was found that signals over periods of more than 2 h displayed a normalized cross-correlation greater than 0.9999 at zero-lag. This provides with a reasonable confidence in the relevance of the invariance postulate.

However, experiments always include noise and most of the time, our knowledge of the signals or spectra is only discrete. Besides, deconvolution is a rather numerically unstable process, requires a lot of care and is not always possible [12,13]. Different algorithms have been used, relying on Fourier transform [14], lineshape interpolation [15–22], etc. We concentrate here on the line barycentre (also called center of mass, or centroid) calculation, which is commonly used .

The use of the line barycentre (also called center of mass or centroid) is a simple solution which is not computer-intensive and is stable under proper conditions. The barycenter actually corre-

sponds to the "mean" of the line: The first moment μ_1 of the line about the centroid is zero. Assuming the lineshape does not vary, the center of mass reflects exactly any translation of the line. What follows describes the possible uncertainties going along with a centroid computation.

Assuming the signal is sampled, one collects data at points i, which have a time or frequency value X_i given by the sampler and an amplitude A_i corresponding to the integrated signal over the dwell time.

Given

$$X_{Bar} = \frac{\sum_i X_i A_i}{\sum_i A_i}. \tag{1}$$

the effect of noise can be assessed from the usual error propagation formula:

$$\sigma^2_{X_{Bar}} = \sum_i \left(\frac{\partial X_{Bar}}{\partial A_i}\right)^2 \sigma^2_{A_i} + 2\sum_{i,j} \frac{\partial X_{Bar}}{\partial A_i}\frac{\partial X_{Bar}}{\partial A_j}\sigma_{A_i A_j} \tag{2}$$

If one assumes a white noise, each point in the spectrum is independent from another and the covariance terms vanish. One can express the partial derivatives as

$$\frac{\partial X_{Bar}}{\partial A_i} = \frac{\sum_j (X_i - X_j)A_j}{\left(\sum_j A_j\right)^2}\sigma^2_{A_i}, \tag{3}$$

Hence the variance on X_{Bar}:

$$\sigma^2_{X_{Bar}} = \sum_i \left[\frac{\sum_j (X_i - X_j)A_j}{\left(\sum_j A_j\right)^2}\right]^2 \sigma^2_{A_i}, \tag{4}$$

or, assuming white noise ($\sigma_{A_i} = \sigma_{A_j} = \sigma_A$),

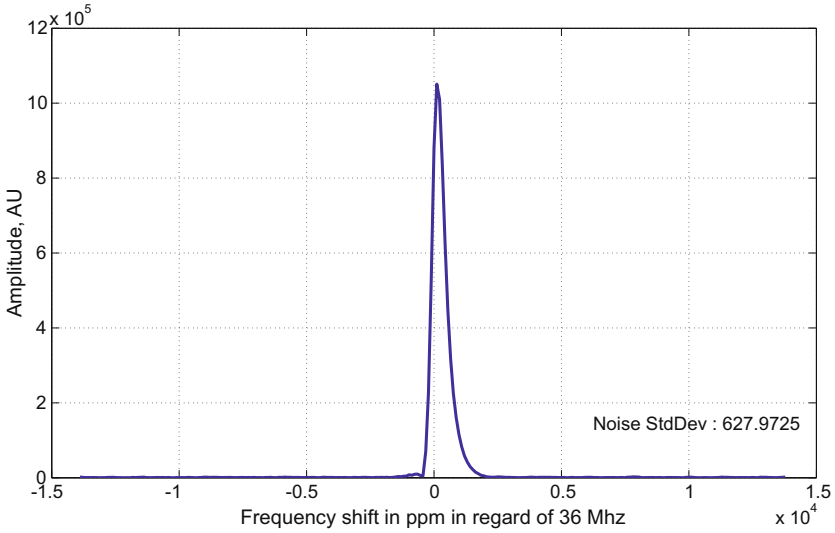

Fig. 6. Typical lineshape recorded during a Hahn echo experiment on liquid ^{3}He in the inhomogeneous test magnet. The lineshape is dominated by the inhomogeneities of the field.

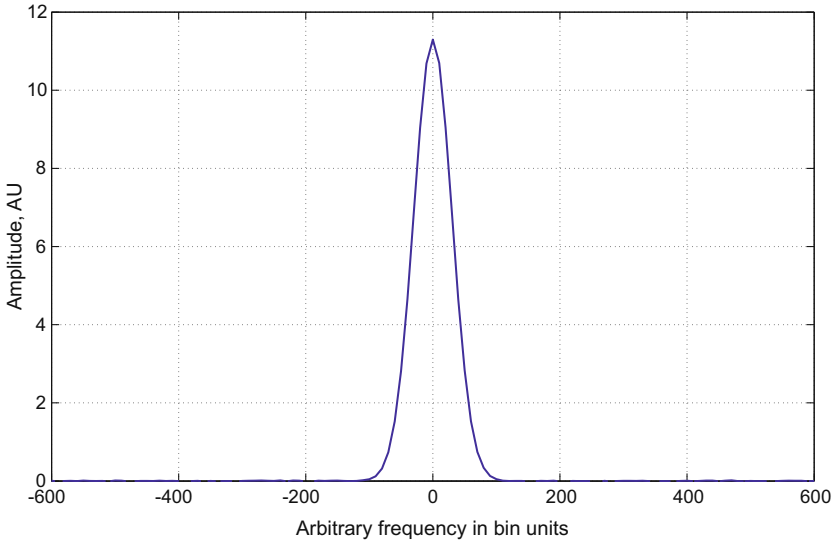

Fig. 7. Gaussian lineshape used to simulate centroid errors. The number of samples on the peak is similar to the number of points on the experimental data. White Gaussian noise with similar standard deviation to the experimental data has been added.

$$\sigma_{X_{Bar}} = \sqrt{\sum_i \left[\frac{\sum_j (X_i - X_j) SNR_j}{\left(\sum_j \frac{1}{SNR_j} \right)^2} \right]^2}, \quad (5)$$

where $SNR_j = \frac{A_j}{\sigma_A}$.

This shows the expected fact that the better the SNR, the better the precision. The latter derivation provides a mean to assess the effect of noise on the uncertainty on the center of mass (or barycenter). Given the level of noise encountered ($\sigma \approx 630$ for a signal at about 5×10^5), the expected error with 3σ confidence interval is about 3.25 ppm. However, noise is not the only source of uncertainty in such a computation. Another uncertainty comes from the sampling itself, or also called "binning". We only know average values of the signal over the dwell time τ at discrete times t_i.

$$\bar{s}(t_i) = \frac{1}{\tau} \int_{-\frac{\tau}{2}}^{\frac{\tau}{2}} s(t_i + \xi) d\xi \quad (6)$$

This binning in time domain results in a binning in the frequency domain. For a signal sampled over a time T, the value in each bin of the frequency domain can be represented as follows:

$$\bar{S}(f_i) = \frac{1}{T} \int_{-\frac{T}{2}}^{\frac{T}{2}} S(f_i + v) dv, \quad (7)$$

where S is the Fourier transform of s. As a result, the calculated barycentre of the line is rather:

$$f_{Bar} = \frac{\sum_i f_i \bar{S}(f_i)}{\sum_i \bar{S}(f_i)} = \frac{\sum_i f_i \frac{1}{T} \int_{-\frac{T}{2}}^{\frac{T}{2}} S(f_i + v) dv}{\sum_i \frac{1}{T} \int_{-\frac{T}{2}}^{\frac{T}{2}} S(f_i + v) dv} \quad (8)$$

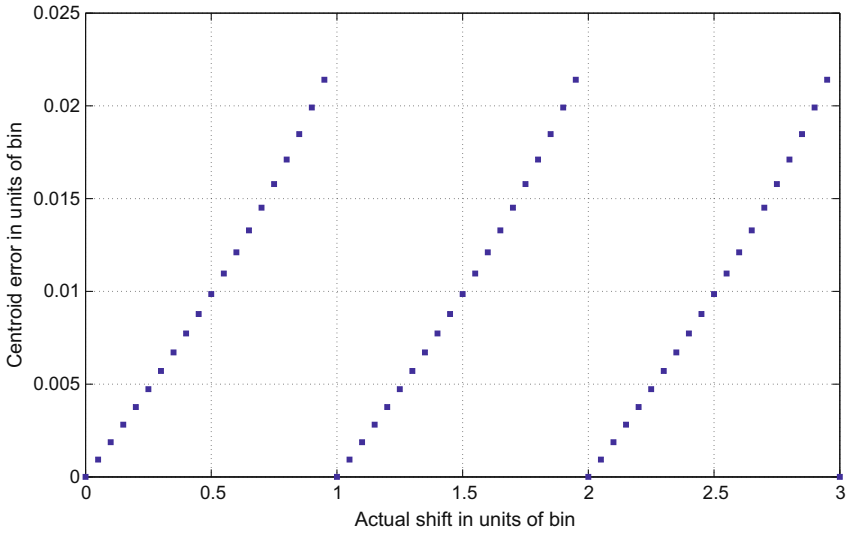

Fig. 8. Computed centroid error in function of the line shift for a noiseless signal. The lineshape is first shifted in its analytical expression and then sampled to simulate the shift of a continuous signal that is sampled. One can notice the periodicity of the error as once one has shifted the line by an integer number of bin, the sampling of the line is exactly the same as the initial one.

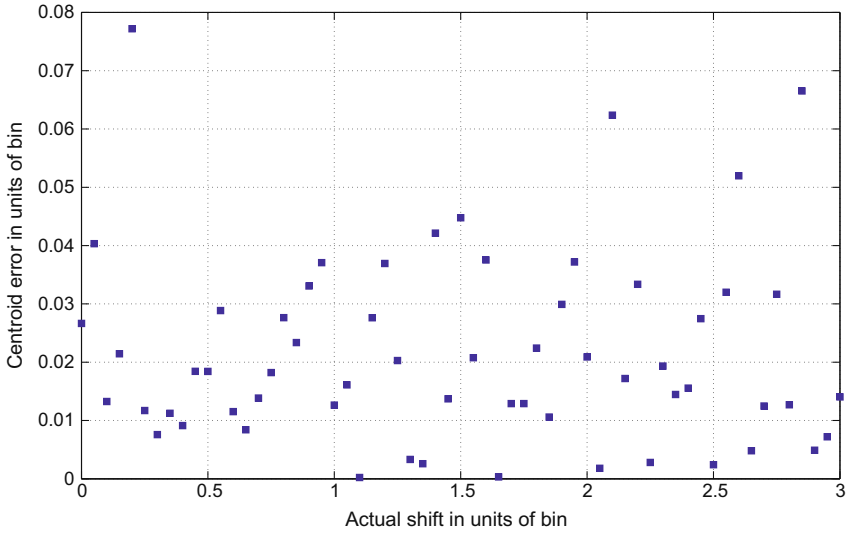

Fig. 9. Centroid error in function of the line shift, in presence of noise, for the optimal window width. The lineshape is first shifted in its analytical expression and then sampled to simulate the shift of a continuous signal that is sampled. A Gaussian noise is then added, with a standard deviation comparable to the experimental noise. The results show that the noise dominates the error on the centroid. However, the error is greater than the one expected from error propagation calculations: the sampling increases the effect of noise on the error.

Following the demonstration of Sheppard's correction [23], we can use a version of the Euler–Maclaurin sum formula, that is, for a function $y(x)$ with $2m$ derivatives,

$$\frac{1}{h}\int_a^b y(x)dx = \sum_{j=1}^{n} y\left(a+\left(j-\frac{1}{2}\right)h - \sum_{j=1}^{m} \times \frac{h^{2j-1}}{(2j)!}B_{2j}\left(\frac{1}{2}\right)\left[y^{(2j-1)}(x)\right]_a^b - S_{2m}, \quad (9)$$

where $y^{(r)}$ is the rth derivative of y, $B_{2m}\left(\frac{1}{2}\right)$ is the value of the $2m$'th Bernoulli polynomial for argument $\frac{1}{2}$ and S_{2m} is a remainder term that can be expressed as

$$S_{2m} = \frac{nh^{2m}}{(2m)!}B_{2m}\left(\frac{1}{2}\right)y^{(2m)}(a+nh\theta), \quad 0<\theta<1. \quad (10)$$

As we are interested in the first moment of the function studied, we put

$$y(x) = x\int_{-\frac{h}{2}}^{\frac{h}{2}} f(x+\xi)d\xi$$

in Eq. (9), which yields the "binned" first moment as

$$\begin{aligned}\bar{\mu_1} &= \frac{1}{h}\int_a^b x\int_{-\frac{h}{2}}^{\frac{h}{2}} f(x+\xi)d\xi dx + R_{2m}\\ &= \frac{1}{h}\int_a^b \int_{-\frac{h}{2}}^{\frac{h}{2}} (u-\xi)f(u)d\xi du + R_{2m}\\ &= \frac{1}{2h}\int_a^b \left[\left(u-\frac{h}{2}\right)^2 - \left(u+\frac{h}{2}\right)^2\right]f(u)du + R_{2m}\\ &= \frac{1}{2h}\left(\mu_2\left(\frac{h}{2}\right) - \mu_2\left(-\frac{h}{2}\right)\right) + R_{2m}\\ &= \mu_1 + R_{2m},\end{aligned}$$

where $\mu_k(m) = \int_a^b (x-m)^k f(x)dx$ and R_{2m} stands for the sum of S_{2m} and the second right-hand term of Eq. (9). Hence, the binned mo-

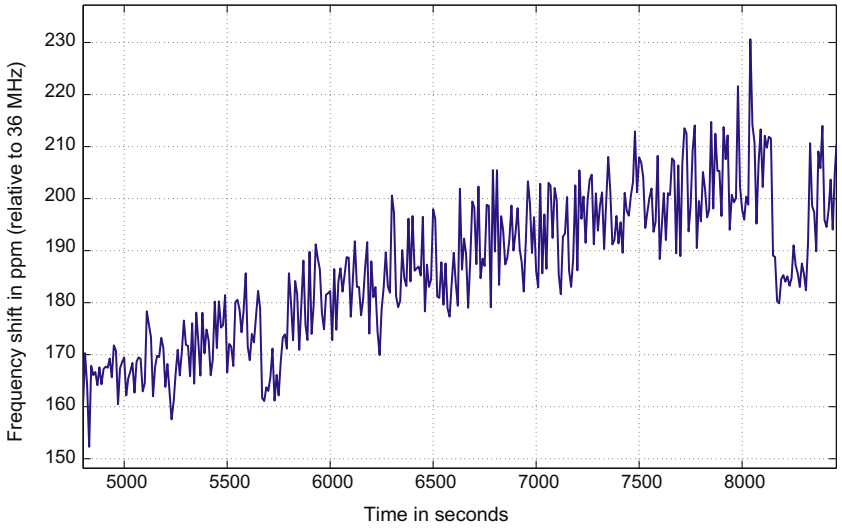

Fig. 10. Measurement of the magnetic field through the NMR signal of liquid ^{3}He. The time evolution of the center frequency when the power supply is acting alone is shown. The drift is greater than 50 ppm/h. This matches the specifications (about 30 ppm/h in the experimental conditions) of the power supply as it is working at less than 10% of its capacity.

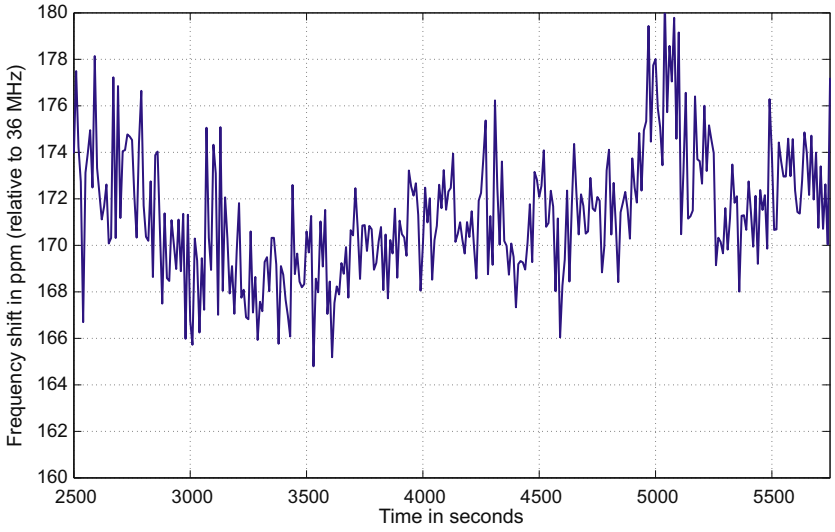

Fig. 11. Measurement of the magnetic field through the NMR signal of liquid ^{3}He. The time evolution of the center frequency with the stabilization system enabled is shown. The efficiency of the stabilizing system is demonstrated with the reduction of the drift to about 15 ppm/h.

ment is equal to the exact moment plus a correction term that only depends on the shape of the line. One can expect that the more points are used, the better it will be. However, it really is the *number of points on the line* that matters. In a signal flawed with noise, low amplitude points will have a lower signal to noise and hence will introduce errors and one should not give in the temptation of using points too far in the tail of the line. As a result, it seems appropriate to use a window to select a useful part of the line in order to obtain the highest accuracy. When designing the acquisition sequence, one should use long dwell times in order to decrease the detection bandwidth to a few times the linewidth and the acquisition duration should be increased as long as the signal has not decayed. This will insure a high number of points on the line. It should also be emphasized that the phase of the signal varies with the center frequency of the line, as the difference between the pulse frequency and the resonance frequency varies. As a result, each spectrum should be phased individually if one wants to use the real or imaginary part of the spectrum. However, this can induce errors as the postulate of invariant lineshape is not satisfied. It is hence more reliable to use the magnitude of the signal, which is free of phase variations and insures the lineshape is not changing.

To assess the error associated with binning, we simulated subbin shift of a Gaussian lineshape (Fig. 7) "similar" to the experimental lineshape (Fig. 6): It features about the same numbers of sample points as the experimental data. The simulation was performed with and without noise, the level of noise being similar to the one encountered during the experiment. For a perfect signal without noise, one can use every single point in the data set and the expected accuracy is less than 2.5% of a bin width. The error is periodic, as the line sampling is exactly the same once it has shifted by an integer number of bin (see Fig. 8). However, in presence of a noise comparable to the one that was encountered during this experiment, the optimum window is about four times the FWHM of the line while the average error is about 5% of a bin width (see Fig. 9). This results in an expected uncertainty of 5.5 ppm on the relative center of the line. This is still one order of magnitude higher than the desired stability of the field. However, we will see in the following that this was sufficient in the context of this experiment.

5. Conclusions

Several series of long-term measurements (several hours of acquisition) were carried on. The measurements processed following the method described above yielded an effective drift of 40 ppm/h for the power supply acting alone (see Fig. 10) while the stabilization system proved itself to improve the stability to about 10 ppm/h (see Fig. 11).

The power supply used to drive the magnet was specified as stable to about 2 ppm/h for a nominal current of 1500 A. The magnet was actually operated at a nominal field of about 1 T, corresponding to a nominal current of about 65 A. This results in an expected stability of about 40 ppm/h. As we resolved this drift (Fig. 10), the observed drift reduction when the stabilization system is engaged proves its efficiency (here a reduction of a factor 4, a little more than the designers were expecting [2]). However, the useful 0.05 ppm/h stability remains to be demonstrated. Another experiment on a larger scale magnet in higher field and room-temperature condition will be conducted to validate the stability at full capacity of the power supply.

To conclude, we described in this paper a method to perform NMR measurements on limited-volume samples in a very low temperature environment and in an inhomogeneous field. These NMR measurements provide with the ability to measure the static field. This method, along with the sample of choice (^{3}He) provided a strong signal, which was suitable for an appropriate signal processing permitting an improvement in resolution. Consequently, we achieved an improvement in resolution by more than an order of magnitude. We also reported T_1 and T_2 values for liquid ^{3}He and pointed out the problem of the diffusion of the sample in and out of the detection coil. This issue will be the object of further investigations in the future.

Acknowledgments

We would like to thank Bruno Coltrinari, the glass blower of SCM who made the quartz cell, Armand Sinnana, Thierry Schild, Jean-Marc Gheller, Stephane Bermond from CEA/IRFU for their participation and expertise on cryogenics and magnets, Patrick Parri from CEA/SPEC for helping us with ^{3}He, and Francesca d'Amico for her help with additional verification experiments. The research leading to these results has received funding from the European Research Council under the European Community's Seventh Framework Programme (FP7/2007-2013), ERC grant agreement 205119 and from the Agence Nationale de la Recherhce contrat ANR-06-JCJC0061.

References

[1] P. Vedrine, G. Aubert, J. Belorgey, J. Beltramelli, C. Berriaud, P. Bredy, P. Chesny, A. Donati, G. Gilgrass, G. Grunblatt, F.P. Juster, F. Molinie, C. Meuris, F. Nunio, A. Payn, L. Quettier, J.M. Rey, T. Schild, A. Sinanna, The whole body 11.7 T MRI magnet for Iseult/INUMAC Project, IEEE Trans. Appl. Superconduct. 18 (2008) 868–873.
[2] A. Sinanna, S. Bermond, A. Donati, P. Gros, C. Hugon, J.-F. Jacquinot, M. Lakrimi, D. Sakellariou, T. Schild, P. Tixador, Field stabilization of an MRI magnet operating in driven mode, IEEE Trans. Appl. Superconduct. 19 (2009) 2301–2304.
[3] D.L. Olson, T.L. Peck, A.G. Webb, R.L. Magin, J.V. Sweedler, High-resolution microcoil ^{1}H NMR for mass-limited, nanoliter-volume samples, Science 270 (1995) 1967–1970.
[4] D. Sakellariou, G.L. Goff, J.F. Jacquinot, High-resolution, high-sensitivity NMR of nanolitre anisotropic samples by coil spinning, Nature 447 (2007) 694–697.
[5] F.J. Low, H.E. Rorschach, Nuclear spin relaxation in liquid helium 3, Phys. Rev. 120 (4) (1960) 1111–1119.
[6] J. Wilks, The Properties of Liquid and Solid Helium, Clarendon Press, Oxford, 1967.
[7] F.E. Terman, Electronic and Radio Engineering, McGraw-Hill, New York, 1955.
[8] E.L. Hahn, Spin echoes, Phys. Rev. 80 (4) (1950) 580–594.
[9] H. Carr, E.M. Purcell, Effects of diffusion on free precession in nuclear magnetic resonance experiments, Phys. Rev. 94 (3) (1954) 630–638.
[10] S. Meiboom, D. Gill, Modified spin-echo method for measuring nuclear relaxation times, Rev. Sci. Instrum. 29 (8) (1958) 688–691.
[11] M. Goldman, Quantum Description of High-resolution NMR Liquids, 2002nd ed., Oxford University Press, 1988.
[12] Y.G. Biraud, Les méthodes de déconvolution et leurs limitations fondamentales, Rev. Phys. Appl. 11 (2) (1976) 203–214.
[13] M. Goez, R. Heun, Reference deconvolution in the frequency domain, J. Magn. Reson. 136 (1999) 69–75.
[14] G.A. Morris, Compensation of instrumental imperfections by deconvolution using an internal reference signal, J. Magn. Reson. 80 (1988) 547–552.
[15] Y. Goto, New interpolation formulas for apodized, magnitude mode fourier transformed spectra, Appl. Spectrosc. 44 (8) (1990) 1386–1390.
[16] Y. Goto, Effects of noise on the interpolation accuracy for apodized FFT spectra of time-domain damped signals, Appl. Spectrosc. 49 (12) (1995) 1776–1780.
[17] Y. Goto, Highly accurate frequency interpolation of apodized FFT magnitude-mode spectra, Appl. Spectrosc. 52 (1) (1998) 134–138.
[18] A. Serreqi, M.B. Comisarow, Frequency interpolation of discrete, apodized, magnitude lineshapes, Appl. Spectrosc. 41 (2) (1987) 288–295.
[19] F.R. Verdun, C. Giancaspro, A.G. Marshall, Effects of noise, time-domain damping, zero-filing and the FFT algorithm on the exact interpolation of fast fourier transform spectra, Appl. Spectrosc. 42 (5) (1988) 715–721.
[20] J.P. Lee, M.B. Comisarow, Advantageous apodization functions for magnitude-mode fourier transform spectroscopy, Appl. Spectrosc. 41 (1) (1987) 93–98.
[21] C.D. Keefe, M.B. Comisarow, Exact interpolation of apodized, magnitude mode fourier transform spectra, Appl. Spectrosc. 43 (4) (1989) 605–607.
[22] C. Giancaspro, M.B. Comisarow, Exact inteprolation of Fourier transform spectra, Appl. Spectrosc. 37 (2) (1983) 153–165.
[23] M.G. Kendall, A. Stuart, The Advanced Theory of Statistics, Distribution Theory, third ed., vol. 1, Griffin, 1969.